Hindawi
International Transactions on Electrical Energy Systems
Volume 2022, Article ID 7194119, 16 pages
https://doi.org/10.1155/2022/7194119

Research Article

Analysis and Implementation of Sliding Mode Controller-Based Variable Frequency Drive Using the SCADA System

Belqasem Aljafari,[1] **L. Ashok Kumar**,[2] **V. Indragandhi**,[3] **and V. Subramaniyaswamy**[4]

[1]*Department of Electrical Engineering, Najran University, Najran 11001, Saudi Arabia*
[2]*Department of Electrical Engineering, PSG College of Technology, Coimbatore, India*
[3]*School of Electrical Engineering, Vellore Institute of Technology, Vellore, India*
[4]*School of Computing, SASTRA University, Thanjavur, India*

Correspondence should be addressed to V. Indragandhi; indragandhi.v@vit.ac.in and V. Subramaniyaswamy; vsubramaniyaswamy@gmail.com

Received 13 July 2022; Revised 6 September 2022; Accepted 11 October 2022; Published 18 November 2022

Academic Editor: Sheng Du

Vector control of an asynchronous machine is traditionally accomplished by analogizing it to a separately excited DC machine. It provides decoupled torque and flux control that is perpendicular to each other, ensuring that neither vector interferes with the other. So, despite their close interconnection, torque and speed control are accomplished separately. The rotor flux is aligned with the direct axis of the synchronously rotating reference frame to achieve this. The PI controllers are critical in achieving the variable frequency drive (VFD) desired topology. The system employs three types of controllers: flux, speed, and torque. The flux controller is easy to tune, but the speed and torque controllers are more difficult to tune because the speed controller's output is the torque controller's reference signal. Furthermore, there is no well-defined method for tuning the controllers in a vector control system. However, perfect tuning is required for the machine's better dynamic behavior. It is clear from the above analysis that system identification is critical for tuning PI controllers. However, as an asynchronous machine, obtaining a decoupled system transfer function is extremely difficult. To solve this problem, the proposed system combines a seven-level pulse width modulation (PWM) inverter for vector control of a three-phase asynchronous nonstandard induction machine used in critical applications in nuclear power plants with a sliding mode control technique that eliminates the complexity of PI tuning. A second-order sliding mode controller could be used in the future to reduce the chattering and parameter variation effects. This controller can be enhanced with fuzzy logic principles to make it more robust and reliable, allowing it to be used in future drive designs for high-rating motors with critical applications.

1. Introduction

In many ways, the induction motor outperforms a separately excited DC motor in terms of performance, power-to-weight ratio, high-speed capability, low starting cost, high dependability, and robustness. The DC motor with a converter and a simple controller is the only option for most modern and superior industrial applications. However, DC motor face some unique challenges, such as commuting and maintenance. The DC motor has a few drawbacks, including a low torque-to-weight ratio and a lower unit capacity. AC motors, particularly induction motors, on the other hand, because of their simple and rugged structure, high torque-to-weight ratio, and reliability, are well suited to mechanical drives. Control, however, is extremely difficult due to the combined effect of flux and the torque component of the current. The scalar control only shows the extent of the control variable's variation. To regulate the speed of an induction motor, a variable voltage, variable frequency power source is required. Maintaining the same terminal voltage to frequency proportion is critical in the v/f control procedure. The scalar control procedure has excellent steady-state performance but poor transient performance [1]. Voltage/frequency control keeps the stator flux linkage

in a steady state by preventing flux and torque from decoupling. As a result of the coupling effect, the drive's transient response is poor. By changing both components independently, the induction motor can be considered a separately excited DC motor [2, 3]. The vector control is accomplished by dividing the stator current into two orthogonal components: one is magnetizing current or the flux component of current, which is towards the flux linkage, and the other is the torque component of current, which is perpendicular to the flux linkage. The vector control or field-oriented control method can be divided into two types based on the flux acquisition method: direct and indirect.

Implementing various types of field-oriented control requires a variety of techniques. The majority of the methodologies require an exact estimate of the position of the rotor or speed. It necessitates the use of speed sensors such as shaft-mounted tachogenerators or digital shaft encoders [4, 5]. The speed sensors raise the drive's cost and size, reduce system reliability, and necessitate extra care when measuring noise. The direct field orientation method requires the rotor flux magnitude which is measured by using hall effect sensors or search coils. The performance and accuracy of the drive system are degraded by the hall effect sensors. At slower speeds, assessing rotor flux by integrating open-loop machine voltages is complicated. Indirect field orientation is straightforward and recommended. Its effectiveness is strongly dependent on accurate knowledge of machine parameters. The above issues have been the focus of induction motor control research. Many studies have been published on assessing rotor flux and speed from terminal voltages and currents rather than taking measurements. This removes the flux or speed sensor, allowing for sensor-free control [5–7].

The major problem with terminal quantity-based flux observers is their machine parameter's sensitivity, particularly stator resistance and rotor resistance of the voltage model flux observer and current model flux observer, respectively. To overcome this issue, different control strategies are attempted to enhance the estimation of rotor flux. Some of them are discussed further [8, 9]. The Kalman filter algorithm as well as its modifications are reliable observers for both linear and nonlinear systems. A modified Kalman filter is used to estimate the speed of induction motor drives which uses a vector controller. Unfortunately, this method has a number of drawbacks, including high computational demands and difficult design and tuning procedures. The rotor saliency method is used for determining the rotor position and speed using the signal injection technique. Stator terminals are injected with high-frequency signals. Appropriate signal processing and filtering of the high-frequency stator current detect the saliencies that are induced in the stator model of the induction motor. These techniques have been demonstrated to have the ability for a range of speeds and parameter-insensitive sensorless control, particularly at low speeds.

The inverter switching state is selected based on the flux position and errors in flux and torque, which are obtained in direct self-control (DTC). Fuzzy logic and artificial neural networks (ANN) have recently received a lot of attention to address the issues of nonlinearity and uncertainty of system parameters. The essential features of neural networks are their way to generate good models of nonlinear systems, their decentralized and multithreaded structure, which renders neural-based control methods quicker, their ease of implementation by software or hardware, and their capacity to learn and adapt to the practices of any real process. In the influence of environmental disturbances or when the IFO drive system experiences defective decoupling due to rotor time constant variations, fuzzy controllers have been shown to enhance measurement accuracy [10–12]. Because fuzzy logic and neural networks have better tracking properties than traditional controllers, they are getting popular as estimators and controllers for a wide range of industrial applications.

The vector control's primary goal is to achieve decoupling. Desirable decoupling will not be achieved if the rotor parameters in use in the decoupling control law do not track their true values. Detuning of rotor variables due to a decrease in torque-producing abilities and magnetic saturation occurredby overexcitation reduces the efficiency of the motor drive. The dynamic control properties have also deteriorated. It is possible to achieve decoupling by adjusting parameters in real time, but it is a very difficult and complex process. Various online tuning methods for mitigating the severity of rotor variable variations have been reported. The rotor parameter detuning problem can be solved with a robust control technique. Apart from the aforementioned issue, induction motor drives have a number of other issues that demand the use of a powerful control technique. Load torque disruptions, parameter estimation in the model used in controller design and analysis, and the necessity to track complex paths rather than just step changes are all examples of these [13, 14]. A robust control method is required in these circumstances. One such method is sliding mode control. A sliding mode controller is appropriate for a specific type of nonlinear system. In the existence of modeling errors, parameter changes, and disruptions, this can be used if the upper bounds of their actual values are known. Certain plant uncertainties or the use of a simplified depiction of system dynamics can lead to inaccuracies in modeling. Sliding mode controller design addresses the issue of maintaining stability and performance in the existence of modeling errors in a structured way [15, 16].

The tracking control of motors and robot manipulators with a wide range of mechanical loads is best suited to the sliding mode control. Induction motors, known as actuators, should obey complex paths which are indicated for manipulator movements. When compared to adaptive controllers for parameter estimation, sliding mode controllers have the advantage of being computationally simple and robust to parameter variations. The disadvantage of sliding mode control is that it causes a large and abrupt change in control variables during the process, putting the system under a lot of stress. It also causes the system states to chatter. Soto, Yeung, and Utkin implemented sliding mode control to the induction motor drive. Control methods are applied to an indirect vector-controlled induction machine in a sliding mode for position and speed control. For

induction motor drives, adaptive input-output linearizing control with a sliding mode is addressed. The sliding mode controller is a great pick for dealing with that sort of problem because the amplitude and speed of the motor flux are controlled separately by sliding mode controllers with variable switching gains in this case.

For the speed control of induction machines, traditional control systems such as PI control have been used. Traditional PI controllers are characterized by a large overshoot and a long settling time. To address these issues, sliding mode control has been used to control electrical drive systems. A sliding mode controller (SMC) is a nonlinear, high-speed switching, feedback control strategy for controlling nonlinear plants that is both effective and reliable. The SMC, on the other hand, is prone to chattering due to its discontinuous switching control [17, 18]. In this article, a sliding mode controller is meant to control the speed of an induction motor inputted by a three-phase voltage source multilevel inverter using the space vector pulse width modulation. The proposed method is validated by simulation results. Due to the widespread usage of induction motors in torque-controlled applications, such as electric automobiles, high-precision torque estimation and control of induction motor drives is a crucial study area [19–21].

The chapter describes the modeling of the induction motor, in section 3 the field-oriented control is presented followed by speed estimation is given in section 5. Section 6 discusses the design of the sliding mode controller, section 7 provides the simulation results, and the work is concluded in section 8.

2. Modelling of the Induction Machine

Even though an induction motor's construction is simple because of its nonlinear characteristics and interdependent behavior in the state-space model, the speed control is very complex compared to DC Motors. Modern controllers for AC motor drives have been developed in response to rapid updates and advancements in variable frequency inverters, as well as the application of control theory. Fitting numerical modeling of the motor to upgrade the controller structure is part of the design. A suitable three-phase induction motor model is required to investigate the entire induction motor drive system. The presumption that is considered for modeling induction motor is by disseminating the stator winding to produce MMF sinusoidally in the air gap, equal mutual inductances, and by ignoring voltage and current harmonics, magnetic circuit saturation, hysteresis losses, eddy current losses, and skin effects.

By rotating the reference frame's d-axis and the stationary reference frame's q-axis, the quantities are assumed to be balanced. The inverter's output voltage is

$$\begin{aligned} V_{sd}^{*} &= \left(K_p + K_i\frac{1}{s}\right)\left(i_{sd}^{*} - i_{sd}\right) - \omega_e \sigma L_s i_{sq}^{*}, \\ V_{sq}^{*} &= \left(K_p + K_i\frac{1}{s}\right)\left(i_{sq}^{*} - i_{sd}\right) + \omega_e \sigma L_s i_{sd}^{*} + \omega_e \frac{L_m}{L_r}\varphi_{rd}. \end{aligned} \tag{1}$$

3. The Field Oriented Control

The flux component (d-axis component) of the stator current, ids, is aligned in the direction of rotor flux, and the torque component of the stator current, iqs, is aligned in the direction perpendicular to it to achieve field orientation along the rotor flux. The slip frequency necessary to acquire indirect field orientation is given by

$$\omega_{sl} = \omega_e - P\omega_r = a_5.\frac{i_{qs}}{\varphi_{dr}}, \tag{2}$$

where

$$a_5 = \frac{R_r L_m}{L_r}.$$

Decoupling of torque and flux is assured in field-oriented control, and it can be controlled. The indirect field orientation control, however, is extremely parameter sensitive owing to the existence of the rotor time constant (Rr/Lr) in equation (23). Erratic parameter variations, external load disturbances, and nonlinear dynamics all have a negative impact on the drive system's control performance.

4. Estimation of Speed

It is better to avoid using a speed sensor because of its price, size of the drive, reliability, and immunity to noise. So, designing and implementing shaft sensorless adjustable speed drive have become an emerging research topic. The speed data required in the presented control technique are estimated using the algorithm described in this section. The speed of the motor is determined by the difference between the slip speed and the synchronous speed. Stator flux components are being used to estimate synchronous speed because they have greater accuracy than rotor flux components.

The speed of the rotor is determined by synchronous frequency or slip frequency. The proposed speed estimation scheme anticipates the synchronous frequency, and it is assumed that the slip frequency is a command.

Figure 1(a) shows the components of the rotor flux vector in the stationary reference frame, and from this, the electrical angle of the rotor flux vector is given by

$$\theta_{\varphi r} = \tan^{-1}\frac{\varphi_{\beta r}}{\varphi_{ar}}. \tag{3}$$

The instantaneous angular frequency is given by

$$\omega_e = \dot{\theta}_{\varphi r} = \frac{\varphi_{ar}\varphi_{\beta r} - \varphi_{\beta r}\varphi_{ar}}{\varphi_{ar}^2 + \varphi_{\beta r}^2}. \tag{4}$$

Figure 1(b) shows the components of the stator flux vector in the stationary reference frame, and from this, the electrical angle of the stator flux vector is given by

$$\theta_{\varphi s} = \tan^{-1}\left(\frac{\varphi_{\beta s}}{\varphi_{as}}\right). \tag{5}$$

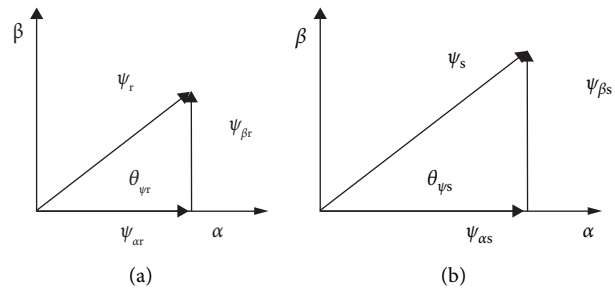

Figure 1: Phasor diagram for rotor and stator flux components.

The instantaneous angular frequency is given by the derivative of this rotor flux angle, which is as follows:

$$\omega_e = \dot{\theta}\varphi_s = \frac{\varphi_{as}\dot{\varphi}_{\beta s} - \varphi_{\beta s}\dot{\varphi}_{as}}{\varphi_{as}^2 + \varphi_{\beta s}^2}. \tag{6}$$

Figure 2 shows a block diagram of the speed estimation method in conjunction with the sensorless speed control scheme.

The derivation helps to design modeling of the induction motor using Matlab Simulink, and it is used for control purposes. The simulation-based models of induction motors with PI control strategies are discussed. In the analytical summary, the induction motor model is provided in an arbitrary reference frame and analyzed in detail. Because vector-controlled drives must be understood and designed using a dynamic model of the machine under control, we derive the conditions for achieving indirect vector control. The speed estimate algorithm is thoroughly explored to deploy the sensorless technique in the current drive system. A brief overview of the multilevel inverter and its type was also discussed, as well as a brief explanation of the cascaded H-bridge inverter and its switching patterns.

5. Design of the Sliding Mode Controller

The derivations of sliding mode surface gain and relevant control laws to determine the speed tracking property are presented in this section. A variable sliding mode control structure is primarily an adaptive nonlinear control that provides stable performance in the face of parameter changes and load torque disturbances. It can be used on either a linear or nonlinear system. The drive reaction is forced to track or slide along a specified trajectory or benchmark model in sliding mode control, despite system parameter variation and load disturbance, using a switching control algorithm. The control DSP identifies the actual trajectory's departure from the reference trajectory and adjusts the switching strategy to restore tracking (Figure 3).

The merits of sliding mode control are system functions similar to a reduced-order system, which is adaptable to parameter variations, implications, and abnormalities, and the time required for convergence is confined. The demerits of sliding mode control are chattering at a high frequency. Because of inertia, the actuator cannot always respond at that speed, and due to irregular input, the structure's cost is considerable. The design of sliding mode control is divided into two stages. The first is the selection of stable hyperplanes in the state/error space on which movement should be governed, referred to as the switching function, and the identified sliding surface is then made appealing by using the suitable control law design in the second step.

An induction motor's mechanical equation is expressed as

$$J\omega_m^* + B\omega_m + T_L = T_e. \tag{7}$$

Here, J is the inertia constant, and B is the viscous friction coefficient of the induction motor; T_L is the external load. ω_m is the rotor mechanical speed in angular frequency, which is proportional to the electrical speed of the rotor $\omega_m = 2\pi\omega p$ where p is the number of poles and T_e is the produced torque of an induction motor. Substituting (8) in equation (34), the mechanical equation becomes

$$\omega_m^* + a\omega_m + f = bi_{qs}, \tag{8}$$

where

$$a = \frac{B}{J},$$

$$b = \frac{K_T}{J}, \tag{9}$$

$$f = \frac{T_L}{J}.$$

The mechanical equation with uncertainties is

$$\omega_m^* = -(a + \Delta a)\omega_m - (f + \Delta f) + (b + \Delta b)i_{qs}, \tag{10}$$

where Δa, Δb, and Δf indicate the uncertainties of the terms a, b, and f, respectively, it should be emphasized that these uncertainties are unknown, and thus determining the upper bound with perfection is tough. The tracking speed error is given by

$$e(t) = \omega_m(t) - \omega_m^*(t). \tag{11}$$

Here, ω_m^* is the speed command of the rotor.

Taking the time derivative of the above equation produced,

$$\dot{e}(t) = \dot{\omega_m} - \omega_m^* = -ae(t) + u(t) + d(t). \tag{12}$$

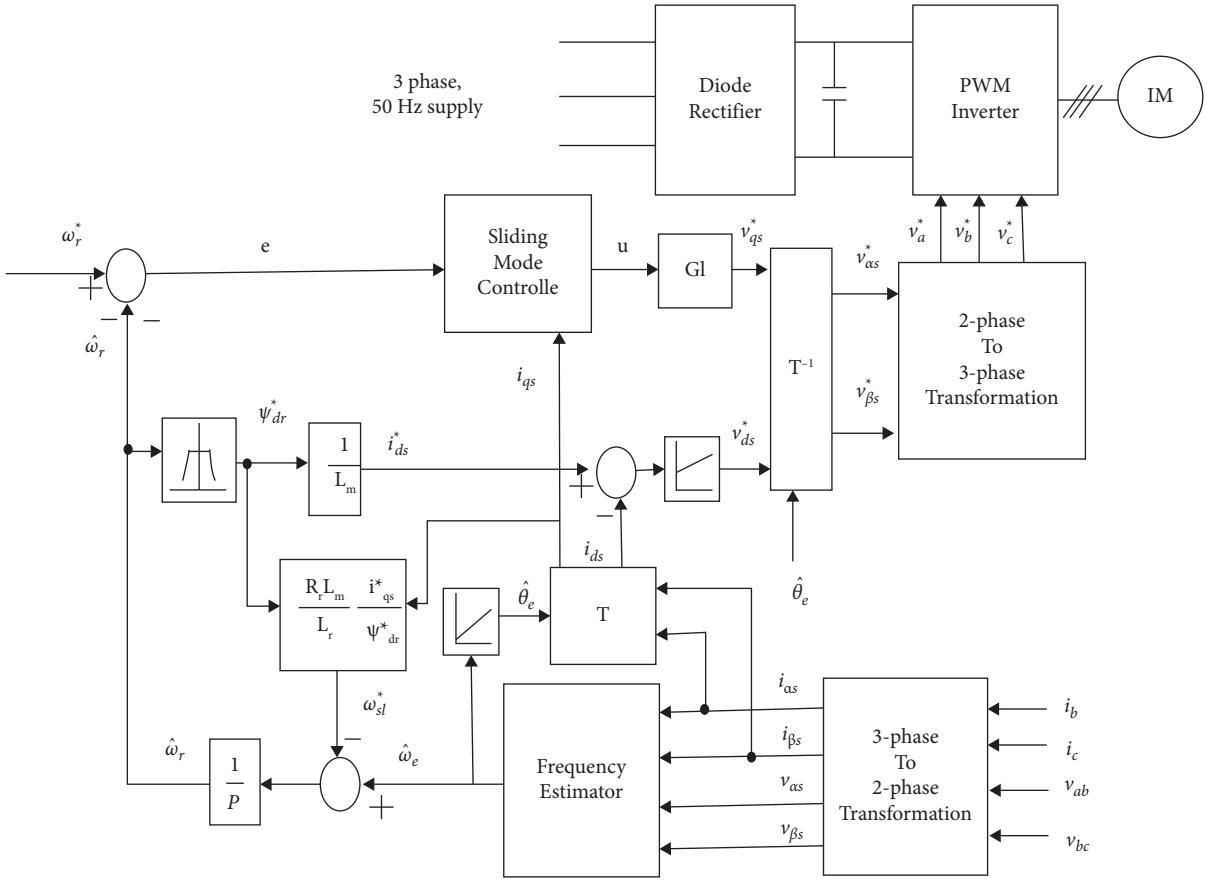

Figure 2: Sensorless speed control scheme for induction motor drive.

Here, the terms listed as follows have been gathered in the signal $u(t)$:

$$u(t) = bi_{qs}(t) - a\omega_m^*(t) - f(t) - \omega_m^*(t). \tag{13}$$

The signal $d(t)$ has been compiled with the uncertainty terms

$$d(t) = -\Delta a\omega_m(t) - \Delta f(t) + \Delta bi_{qs}(t). \tag{14}$$

To compensate for the system's uncertainties, a sliding adaptive control strategy is proposed. In sliding control theory, the switching gain must be built in order to achieve the sliding condition. An appropriate sliding gain needs to be chosen to compensate for the uncertainties in order to achieve this requirement. When choosing the sliding gain vector, an upper bound of parameter fluctuations, unmodeled dynamics, noise magnitudes, and other factors should be known, but these bounds are typically unknown or impossible to compute in practice. Setting the sliding gain to a high enough value could be a solution, but this technique could result in an extremely high control signal and considerably more activity control is required to meet the control aim. One technique to tackle this challenge is to estimate the gain and update it with an adaptation law to achieve the sliding condition.

The sliding variable $S(t)$ is defined with an integral component as

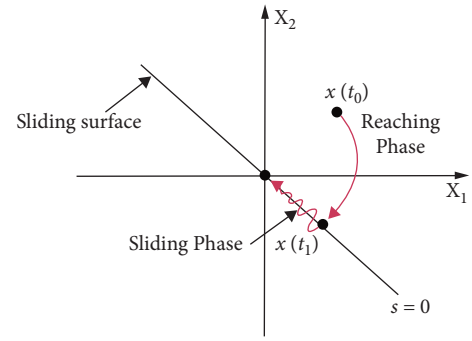

Figure 3: Sliding surface.

$$S(t) = e(t) + \int_0^t (a+k)e(\tau)\mathrm{d}\tau. \tag{15}$$

Here, k is a constant gain and a is a previously defined parameter in equation (36).

The sliding surface $S(t) = 0$ (5.10).

$$u(t) = -ke(t) - \widehat{\beta}(t)\gamma\mathrm{sgn}(S). \tag{16}$$

Here, β is the estimated switching gain, γ is a positive constant, S is the sliding variable defined in equation (42), and *sgn(s)* is the signum function. The switching gain β is adjusted according to the updating law, which is as follows:

$$\widehat{\beta} = \gamma|S|\widehat{\beta}(0) = 0. \tag{17}$$

The error signal is compared to the constant value and reference gain value. With the available value, the comparative function is created and analyzed. As per the theory, the obtained output is compared to the suitable control law and set to zero. The output is made to slide to the determined and designed slide surface when the condition is met.

The simulation provides the simulation-based design of sliding mode control to the induction motor with all supporting gain values. To lessen chattering, a limit layer of width θ is presented on both sides of the sliding line. As a result, the control gain inside the limit layer is reduced, resulting in a smooth control sign. Then, the control law of the equation $i_{qs}^{*} = -K.\mathrm{sgn}(S)$ modifies to the following equation:

$$i_{qs}^{*} = -K.\mathrm{sgn}\left(\frac{S}{\theta}\right),$$

$$\text{where sat}\frac{S}{\theta} = \frac{S}{\theta}\ if\ |S| \le \theta, \tag{18}$$

$$\mathrm{sgn}(S)\ if\ |S| > \theta.$$

To reduce this chattering, the sliding mode controller with a boundary layer as given by the following equation is

$$i_{qs}^{*} = \left\{\frac{\widehat{-G} - \lambda\dot{e} + \ddot{\omega}r^{*}}{\widehat{b}}\right\} - Ksat\left(\frac{S}{\theta}\right). \tag{19}$$

The outline and application of a sliding mode controller for induction motor control are shown. The sliding mode control hypothesis is quickly demonstrated, and the control law is inferred. The controller gain and bandwidth are dictated by several facts such as load variations, different rotor resistance, and so on. To lessen the chattering impact, the control law is altered, and the job summary is so presented (Figure 4).

6. Simulation Results and Discussion

The induction motor is a vertical, single-stage, top suction, free surface pump of a nonstandard machine as perIS325; the odd rating is to mitigate the torque requirement. The ratings of the motor are presented in Table 1.

The motor is mainly used in the core cooling of the nuclear plant, where the liquid sodium is used as a coolant, and the motor is operated at different speeds which are controlled by the drive mechanism. The design calculation for a 7-level cascaded H-Bridge inverter involves the determination of V_{dc} and I_{dc}. For the cascade bridge, a seven-level inverter is given in (Figure 5.). The line voltage and the line current of the inverter are $V_{\mathrm{l}} = 3150$ V and $I_{\mathrm{l}} = 804$ A, respectively. From this, the phase voltage is derived as $V_{\mathrm{p}} = 607$ V. The Vdc = 1206 V, which is 15% more than the phase voltage, and $I_{\mathrm{dc}} = 1206$ A, which is 15 percent more than the phase current. The sim module shows the arrangement of the IGBT cascaded H- bridge 7-level inverter design for the drive system. Each bridge has the value of $V_{\mathrm{dc}} = 909.32$ V and $\mathrm{I_{dc}} = 1206$ A.

The single-phase seven-level inverter output is shown in Figure 6, and the filtered output is shown in Figure 7; the three-phase seven-level inverter output phase voltage fed to an induction motor is shown in Figure 8.

Figure 9 depicts the stator currents in three phases, while Figure 10 depicts the speed variation. The speed rises until it reaches 590 rpm. The voltage and current are FFT-analyzed, and the corresponding spectrums are shown in Figures 11 and 12, respectively. The magnitude of the fundamental voltage for a seven-level inverter-fed induction motor drive is 234.4 Volts, as can be seen. Total harmonic distortion is 3.51 percent, with a fundamental current magnitude of 91.15 Amperes. There is a 1.01 percent total harmonic distortion.

The THD generated by the seven-level inverter with the drive is found to be minimal. The simulation results for voltage, current, speed, and spectrum are shown. This drive system can be employed in industries that demand minimal harmonic output from variable-speed drives. The flux and speed control subsystem is shown in Figure 13 where PI tuning is used to control the speed.

The subsystem provides the control logic for park and clack transformation of the induction motor which provides the theta of the motor (Figure 14).

The inference of the waveform shows the presence of high peak current during starting of the PI tuning method, which is a main drawback in the system and is to be rectified. The current waveform is shown in Figure 15.

This section uses simulation examples to investigate the performance of the adaptive sliding-mode control in the aspect of speed regulation. Figure 16 shows the rotor speed tracking reference. The rotor speed tracks the reference (1500), where it provides smooth speed control.

The Simulink describes the SMC control for the nominal speed of the motor (Figure 17).

The waveform shown in Figure 18 proves that the SMC is robust irrespective of speed variation. When the reference is changed to the nominal speed of the motor, the rotor speed tracks it, which provides the elimination of high peak current while starting and smooth control.

The characteristics of the motor show that the time taken for the SMC control is 56 minutes which, when compared with existing system performance, the time taken is less, which proves that speed is smoothly controlled and, in turn, increases the entire system performance (Figure 19). Hence, the high peak current problem is rectified, and the objective of work is satisfied. Figures 20(a), 20(b) and Figure 21 show the HMI and SCADA screen of the VFD drive panel which gives a detailed description of the system configuration and status of the individual system implemented. The abnormalities are identified easily from the control center. The faculty areas can be separated from the live supply lines. The equipment protection is ensured by taking a quick decision based on the parameters displayed in the panel.

The snapshot provides the information of the drive system in the common control panel (CCP), which shows that the motor is in a running state (Figure 21). The figure is a

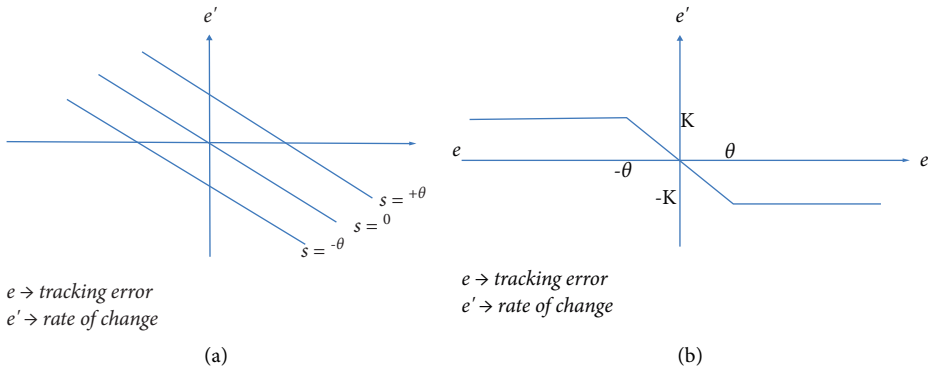

Figure 4: Sliding mode principle with the boundary layer.

Table 1: Ratings of the induction motor.

Sl.No.	Parameters	Values
1.	Voltage	415 V
2.	Star/delta	Star
3.	Pole	10
4.	Rated current	40 A
5.	Nominal speed	590 rpm
6.	Per phase stator resistance	0.0117 Ω
7.	Per phase rotor resistance	0.0234 Ω

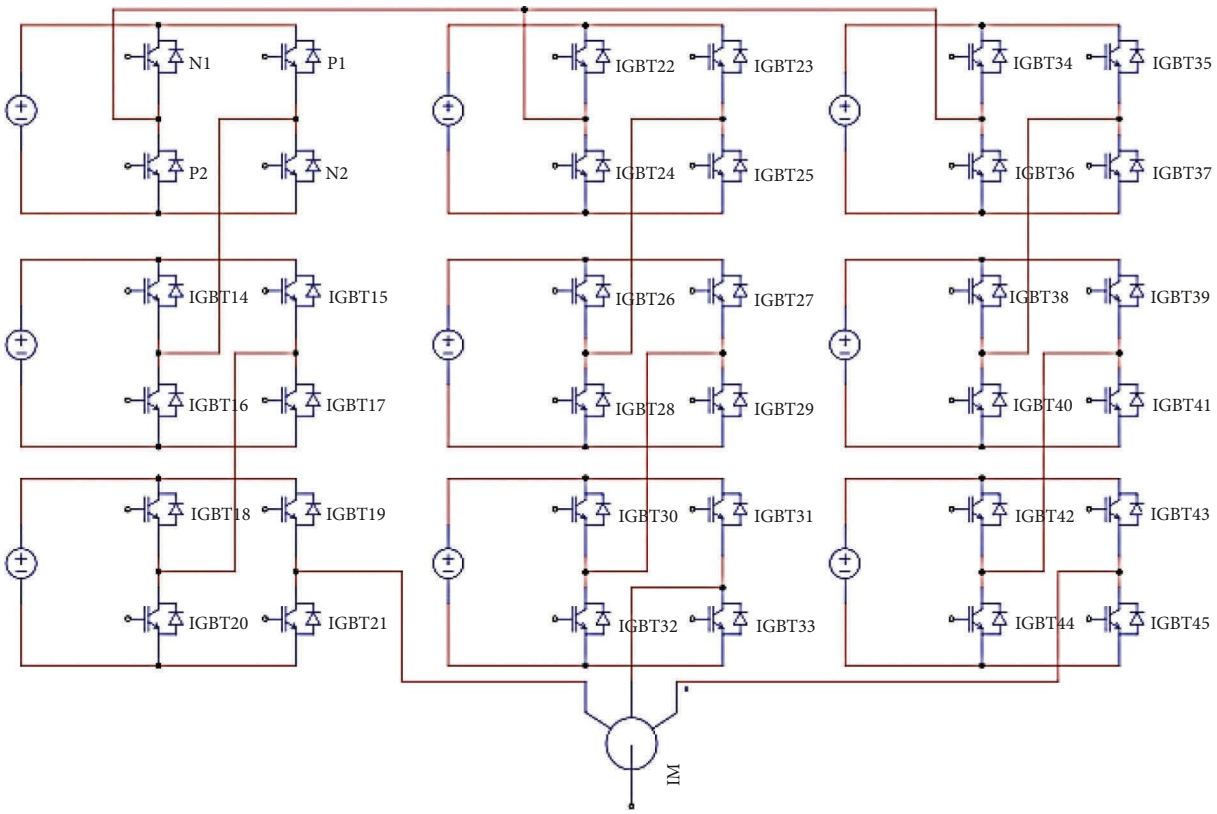

Figure 5: Cascaded H-bridge of seven-level inverter fed induction motor drive.

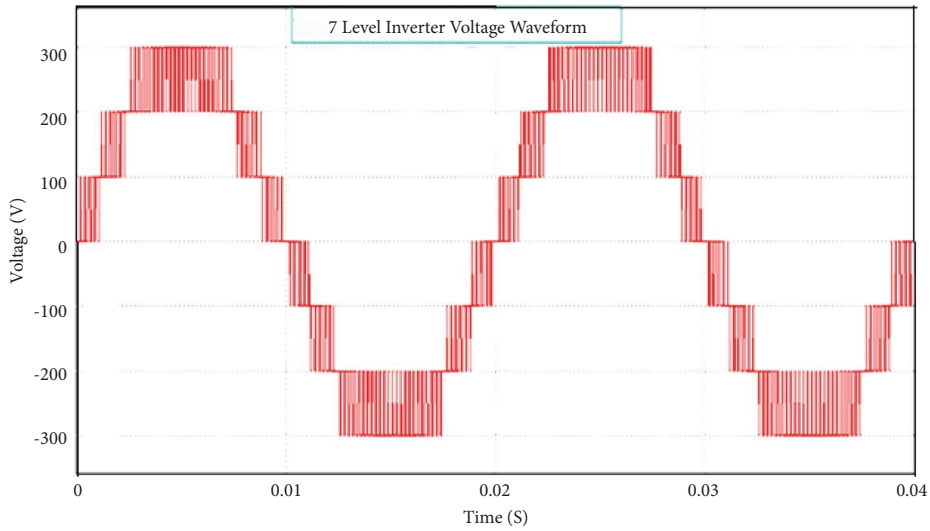

Figure 6: The output voltage waveform of a single-phase seven-level inverter.

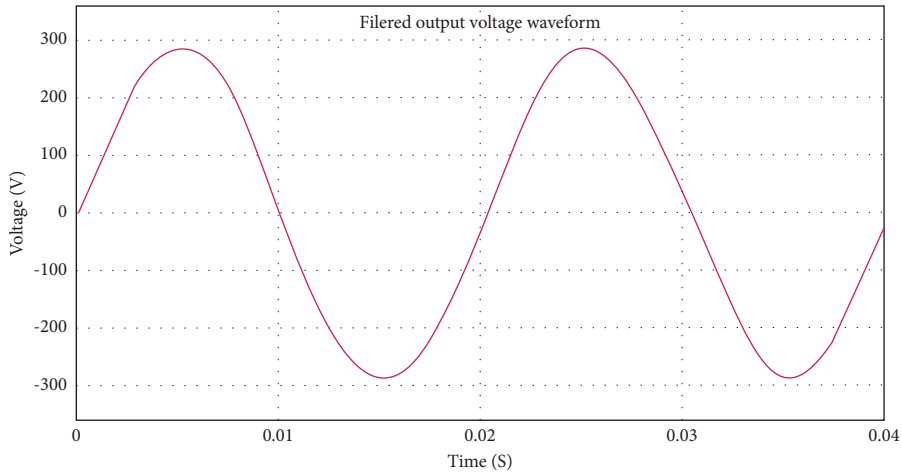

Figure 7: The output voltage waveform of a single phase seven-level inverter with a filter.

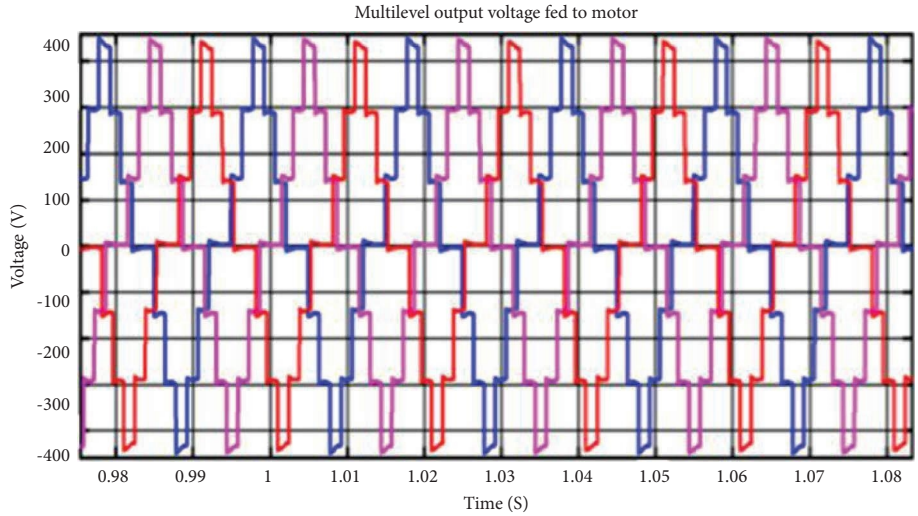

Figure 8: The output waveform of the seven-level inverter is fed to the motor with a filter.

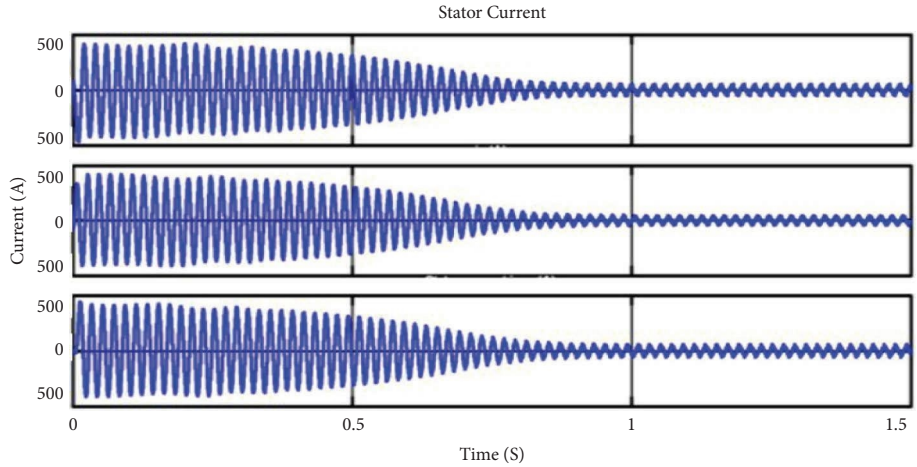

Figure 9: Three-phase stator current.

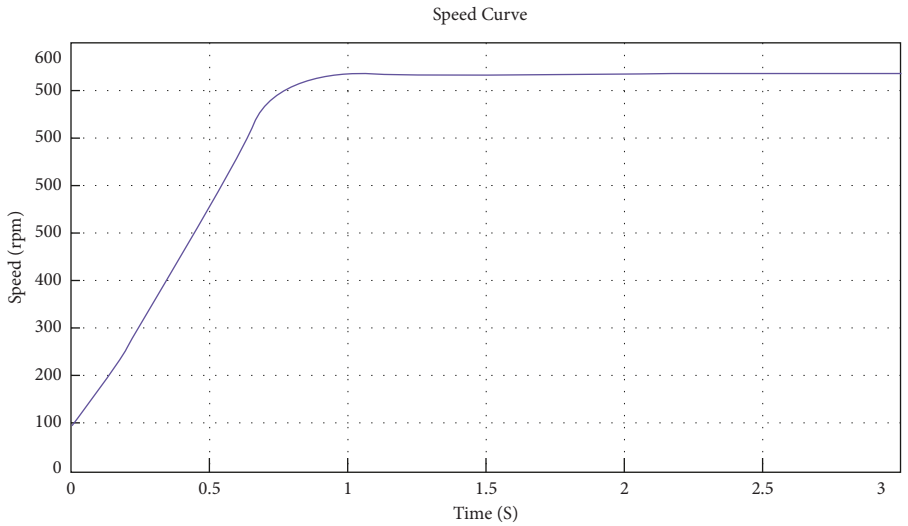

Figure 10: Speed vs time.

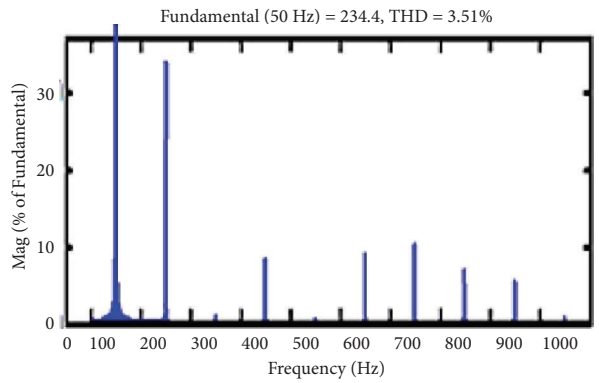

Figure 11: FFT analysis of voltage.

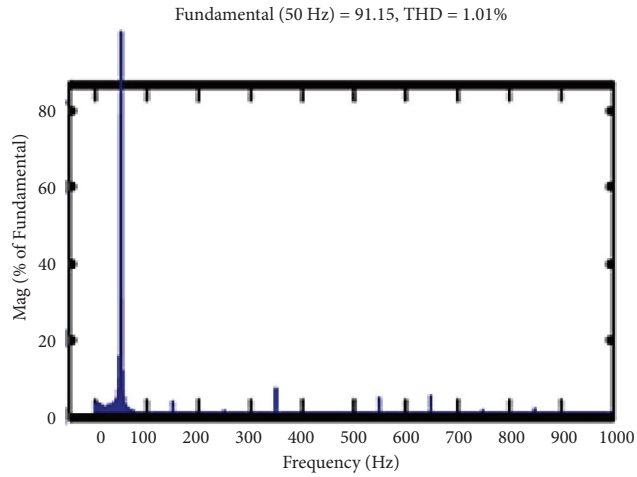

Figure 12: FFT analysis of current.

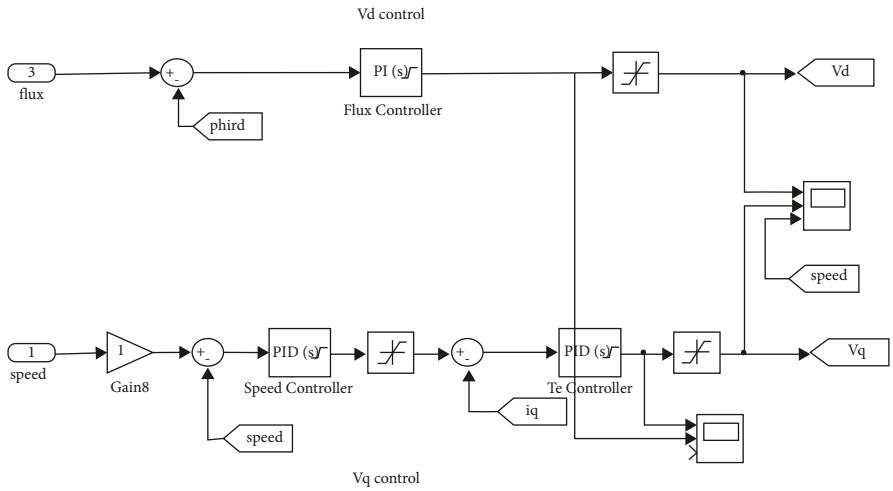

Figure 13: The subsystem of flux and speed control.

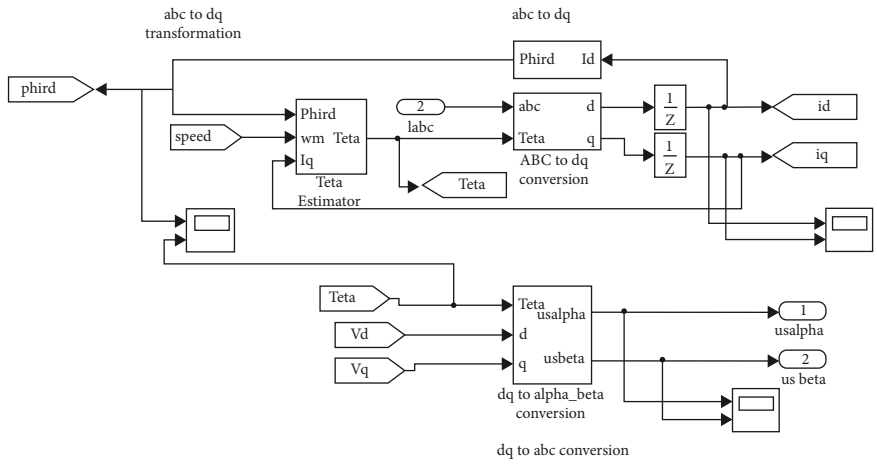

Figure 14: The subsystem of abc to dqtransformation.

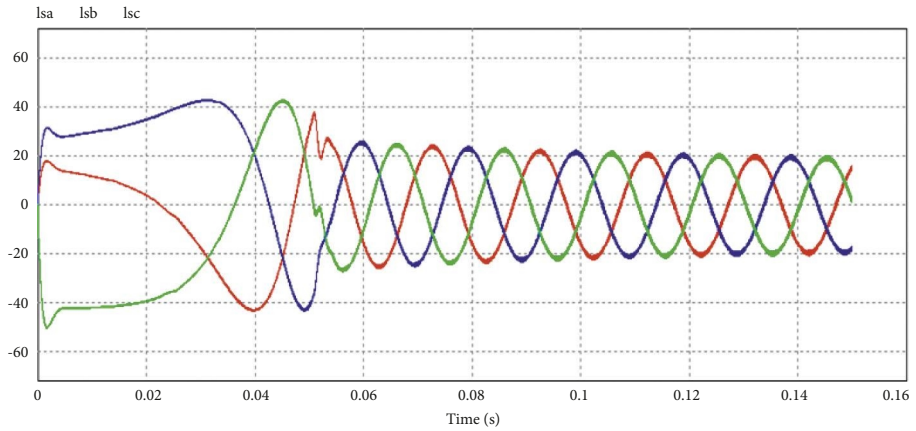

Figure 15: The current waveform of the motor.

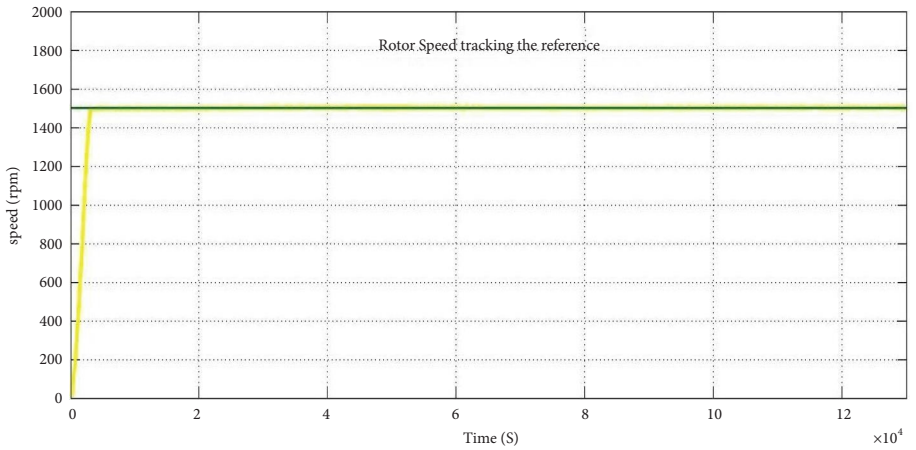

Figure 16: Rotor speed tracking waveform.

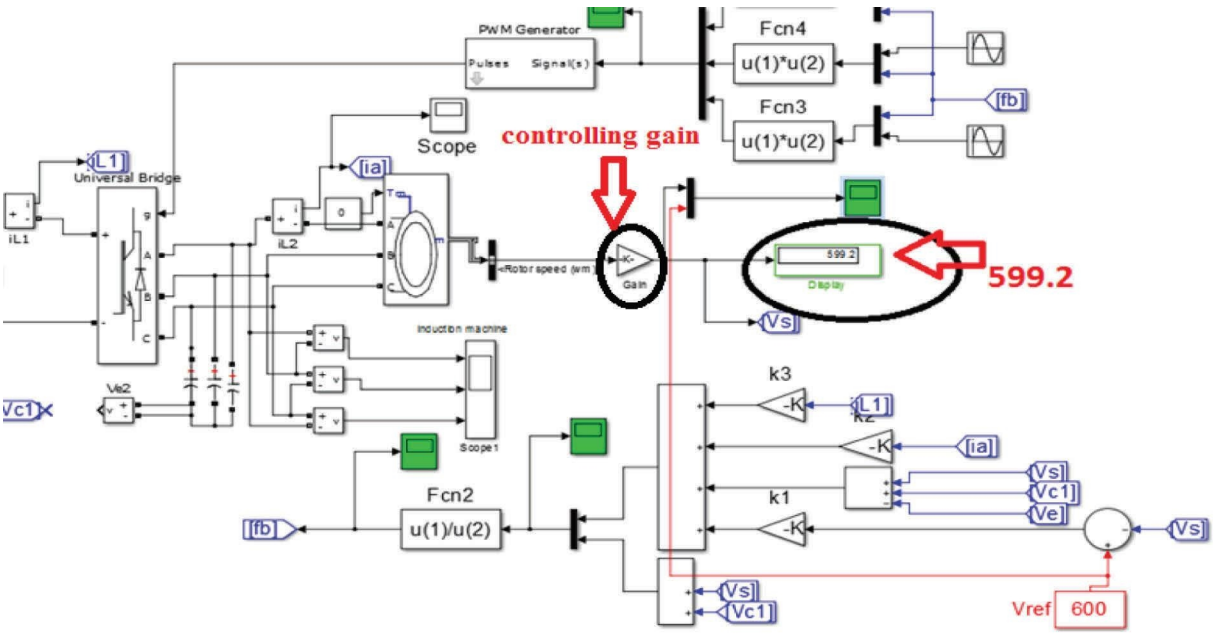

Figure 17: Simulink for SMC control for nominal speed of the motor.

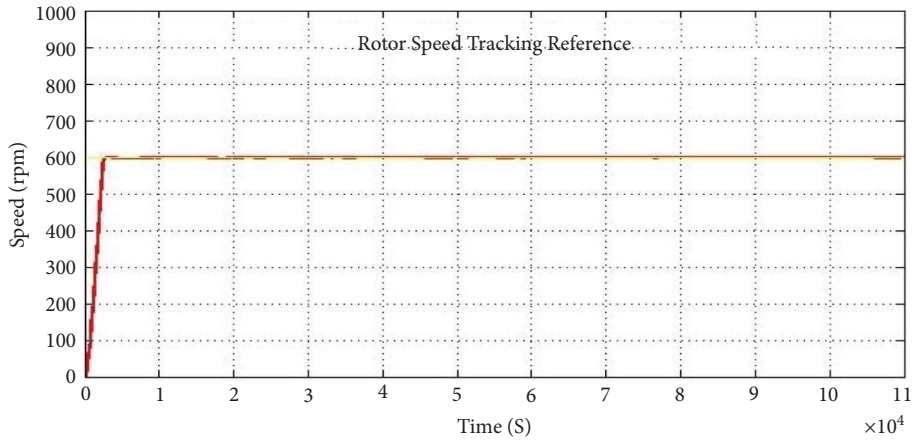

Figure 18: Rotor speed tracking the reference (600) of the nominal speed of the motor.

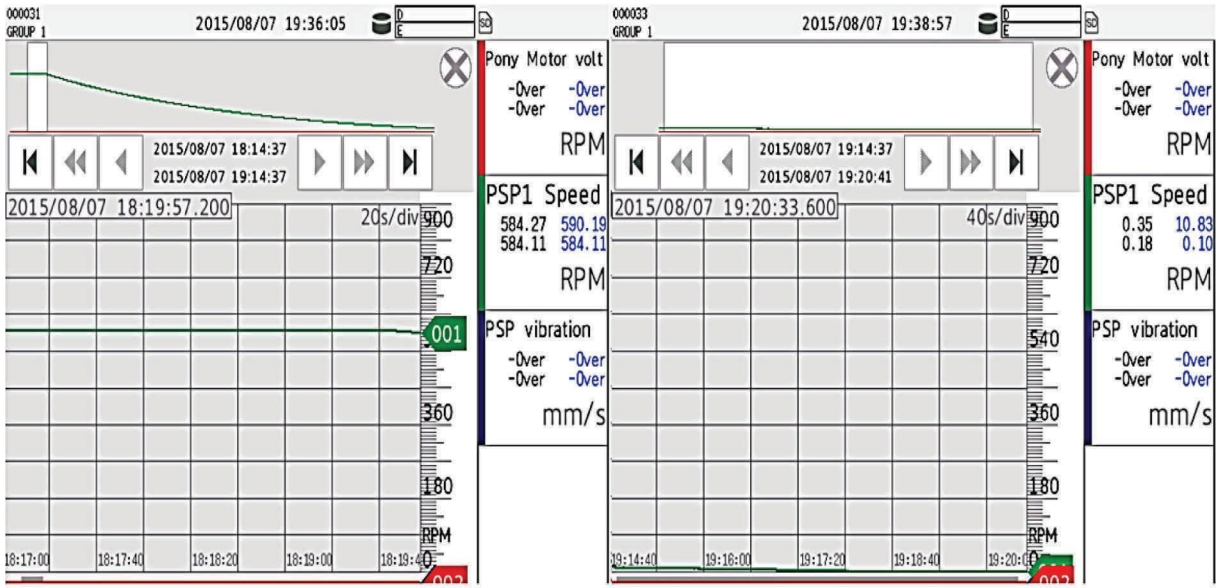

- **Motor coast down time from 590RPM to Zero RPM is 56 Minutes**

Figure 19: Characteristics of the motor with PI and SMC.

complete pictorial representation of the system from supply to drive. The power flow at any instant can be visualized.

The snapshot shown in Figure 22 provides information about the voltage, power, and current values and also gives an indication about the working of the drive system. The functioning of the drive is identified from this screen. The fault in the cooling system, converter, controller, supply, and motor can be observed clearly.

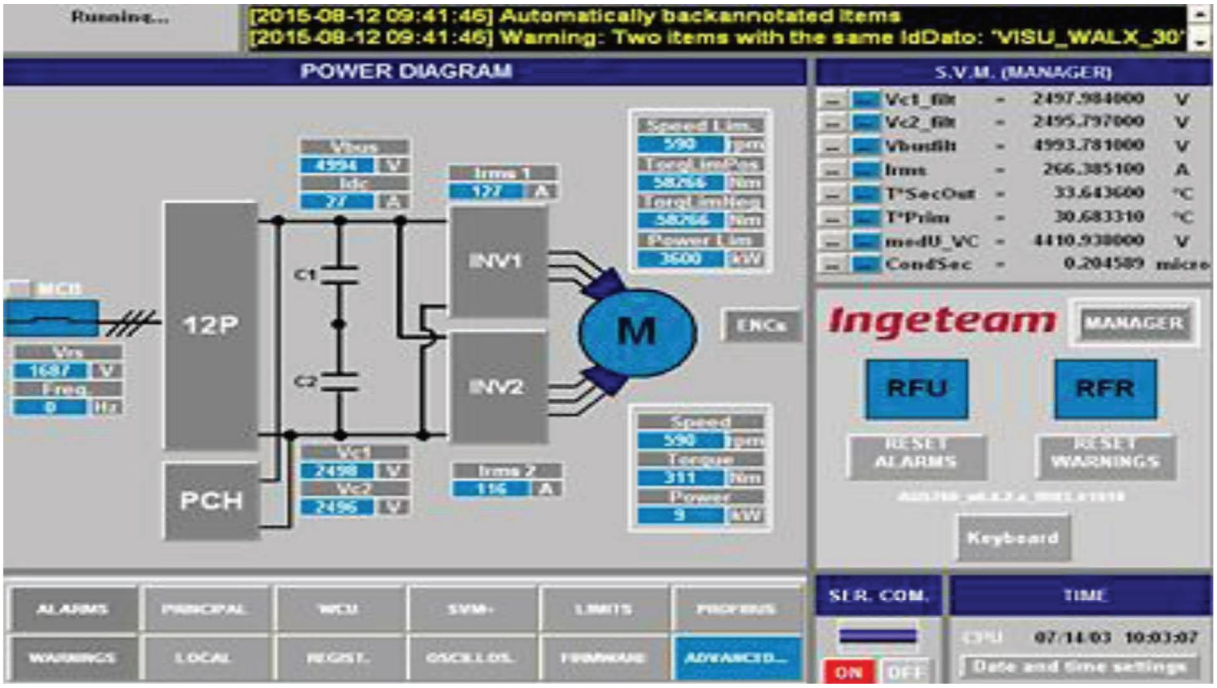

(a)

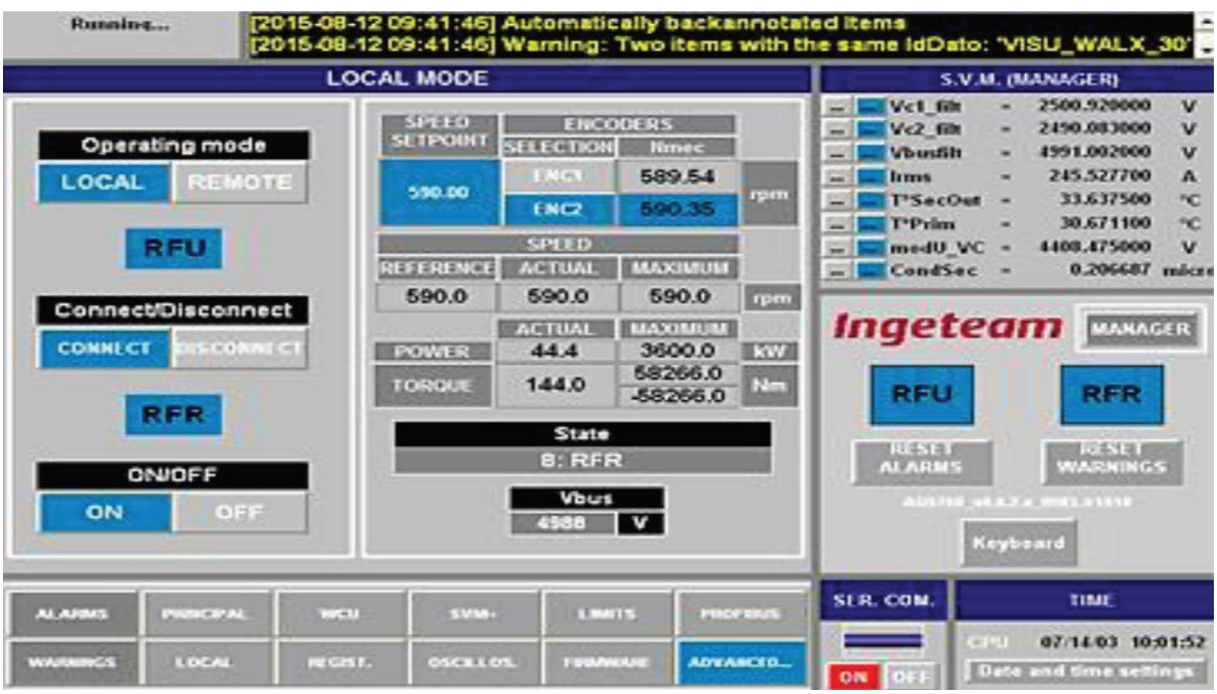

(b)

Figure 20: HMI screen of the VFD panel in the power plant.

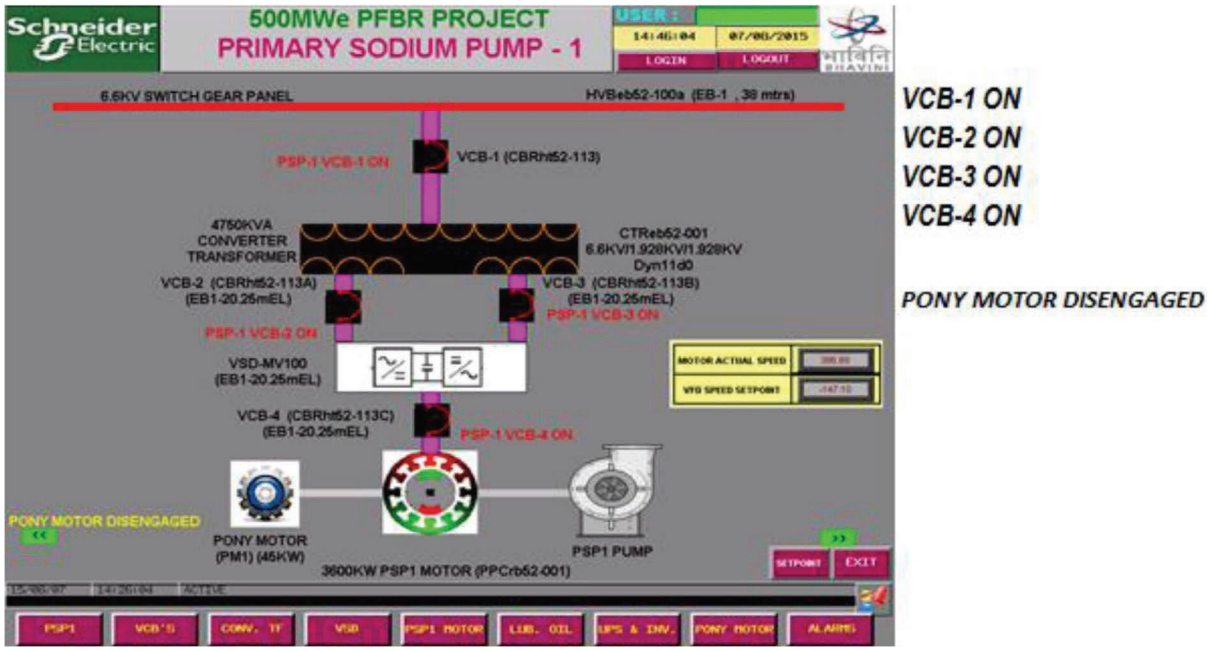

Figure 21: VFD running state screen conditions in the common control panel (CCP).

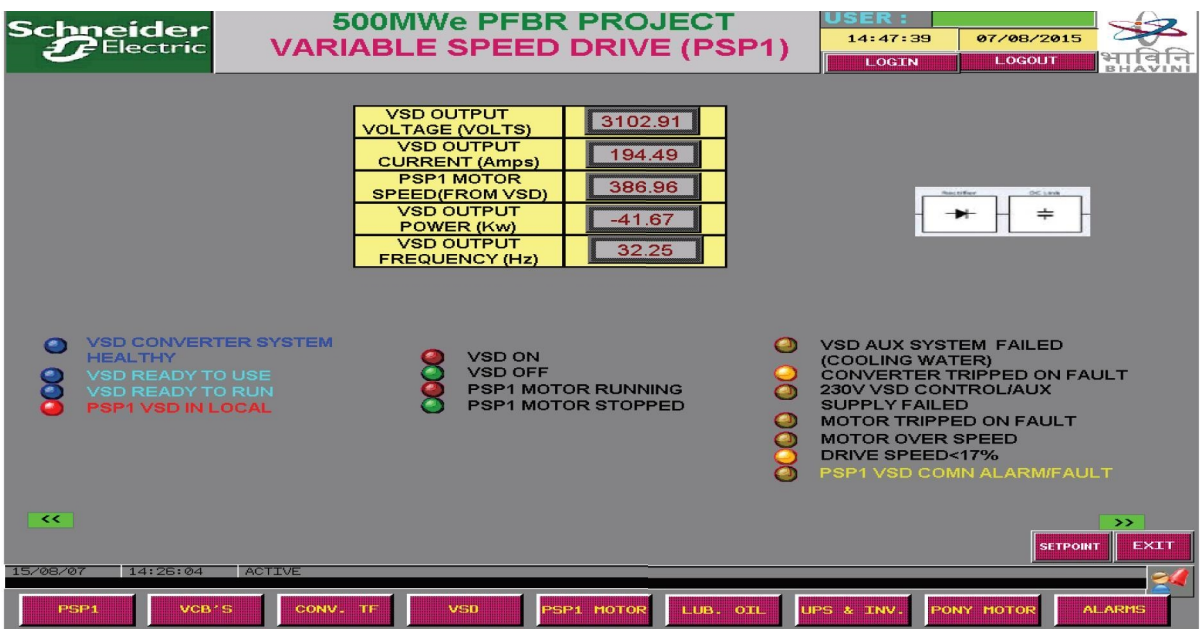

Figure 22: Drive output in SCADA.

7. Conclusion

With progressive technology such as multilevel inverters, problems such as high peak current during motor starting, heating effect, and mismatch of the switching pattern of the existing system were rectified and improved. The dynamic performance of the induction motor drive with an indirect vector controller has been improved with less settling time and zero overshoot by implementing sliding mode control which outperforms traditional PI control. The resiliency of the sliding mode control has been demonstrated during sudden changes in load. The proposed control technique tracks the speed effectively though the load torque, and the parameters are ambiguous. The calculated speed contains ripples due to the discrepancy between current and speed sampling timings. However, the drive system's speed response is acceptable when the predicted speed is used in the control technique. A 2nd order sliding mode controller could be used in the future to reduce the chattering and parameter variation effects. This controller can be enhanced with fuzzy

logic principles to make it more robust and reliable, allowing it to be used in future drive designs for high-rating motors with critical applications in upcoming power plant units.

Abbreviations

DTC: Direct self-control
ANN: Artificial neural networks
SMC: Sliding mode controller
HMI: Human-machine interface
SCADA: Supervisory control and data acquisition
VFD: Variable frequency drive
CCP: Common control panel
THD: Total harmonic distortion
FFT: Fast fourier transform
PWM: Pulse width modulation
MLI: Multilevel inverter

Data Availability

The data used to support the findings of this study are available from the corresponding author upon request.

Conflicts of Interest

The authors declare that they have no conflicts of interest.

Acknowledgments

The authors are thankful to the Deanship of Scientific Research at Najran University for funding this work under the Research Groups Funding Program (NU/RG/SERC/11/6).

References

[1] R. Bharti, M. Kumar, and B. M. Prasad, "V/F control of three phase induction motor," in *Proceedings of the International Conference on Vision towards Emerging Trends in Communication and Networking (ViTECoN)*, Vellore, India, May 2019.

[2] J. M. Pena and E. V. Diaz, "Implementation of V/f Scalar Control for Speed Regulation of a Three-phase Induction Motor," in *Proceedings of the IEEE ANDESCON*, IEEE, Arequipa, Peru, October 2016.

[3] A. R. Harsha, S. Pranupa, B. M. Kiran Kumar, S. Nagaraja Rao, and M. S. Indira, "Arduino based V/f drive for a three phase induction motor using single phase supply," in *Proceedings of the 2020 International Conference on Smart Technologies in Computing, Electrical and Electronics (ICSTCEE)*, IEEE, Bengaluru, India, October 2020.

[4] B. K. Nishad and R. Sharma, "Induction motor control using modified indirect field oriented control," in *Proceedings of the 2018 8th IEEE India International Conference on Power Electronics (IICPE)*, IEEE, Jaipur, India, December 2018.

[5] H. Xie, F. Wang, W. Zhang, C. Garcia, J. Rodriguez, and R. Kennel, "Predictive field oriented control based on MRAS current estimator for IM drives," in *Proceedings of the2020 IEEE 9th International Power Electronics and Motion Control Conference (IPEMC2020-ECCE Asia)*, IEEE, Nanjing, China, November 2020.

[6] A. Paladugu and B. H. Chowdhury, "Sensorless control of inverter-fed induction motor drives," *Electric Power Systems Research*, vol. 77, pp. 619–629, 2007.

[7] Z. Zhang and A. M. Bazzi, "Robust sensorless scalar control of induction motor drives with torque capability enhancement at low speeds," in *Proceedings 2019 IEEE International Electric Machines & Drives Conference (IEMDC)*, IEEE, San Diego, CA, USA, May 2019.

[8] V. J. Stil, K. Miklosevic, Z. Spoljaric, and G. Kurtovic, "Induction motor sensorless and closed loop torque control in frequency converters," in *Proceedings of the 2018 International Conference on Smart Systems and Technologies (SST)*, IEEE, Osijek, Croatia, October 2018.

[9] X. Cui, B. Li, Z. Kou, and Y. Qiao, "Measurement and control system for variable-frequency speed regulating of motor based on PLC and HMI," in *Proceedings of the IEEE 8th Joint International Information Technology and Artificial Intelligence Conference (ITAIC)*, IEEE, Chongqing, China, May 2019.

[10] J. P. Wang, X. L. Meng, S. L. Zhang, and Y. K. Zhu, "Adaptive sliding mode control for an unmanned mini vehicle," in *Proceedings of the2020 5th International Conference on Mechanical, Control and Computer Engineering (ICMCCE)*, IEEE, Harbin, China, December 2020.

[11] Z. Li, X. Li, and B. Cui, "Cloud neural algorithm based load frequency control in interconnected power system," in *Proceedings of the2020 24th International Conference on Automation and Computing (ICAC)*, IEEE, Newcastle Upon Tyne, UK, September 2018.

[12] T. Long, E. Li, Y. Hu et al., "A vibration control method for hybrid-structured flexible manipulator based on sliding mode control and reinforcement learning," *IEEE Transactions on Neural Networks and Learning Systems*, vol. 32, no. 2, pp. 841–852, 2021.

[13] S. S. Kumar Singh, Arkdev, and M. K. Sarkar, "Load frequency control: higher order sliding mode observer based integral higher order sliding mode controller with stochastic perturbation," in *Proceedings of the 2018 2nd International Conference on Power, Energy and Environment: Towards Smart Technology (ICEPE)*, IEEE, Shillong, India, June 2018.

[14] M. Yang, B. Xiaowei, T. Yue, and J. Yuanwei, "Design of sliding mode controller for frequency control in an isolated wind-diesel hybrid system," in *Proceedings of the 2013 25th Chinese Control and Decision Conference (CCDC)*, IEEE, Guiyang, China, May 2013.

[15] J. Robles, F. Sotelo, and J. Chavez, "Robust nonsingular terminal sliding mode control with constant frequency for DC/DC boost converters," in *Proceedings of the 2020 IEEE 21st Workshop on Control and Modeling for Power Electronics (COMPEL)*, IEEE, Aalborg, Denmark, November 2020.

[16] R. R. Vasu, S. G. Fernandez, and K. Vijayakumar, "Enhanced space vector modulated scalar control of induction motor," *Indonesian Journal of Electrical Engineering and Computer Science*, vol. 21, no. 2, pp. 707–713, 2021.

[17] A. Fatima, T. Almas, M. K. A. Biabani, and M. Imran, "Sliding mode control of induction motor used in traction," in *Proceedings of the 2016 International Conference on Electrical, Electronics, and Optimization Techniques (ICEEOT)*, IEEE, Chennai, India, March 2016.

[18] P. Parida, *A Sliding Mode Controller for Induction Motor Drives" Dissertation*, National Institute of Technology, Rourkela, Orissa, 2009.

[19] R. Sreejith and B. Singh, "Sensorless predictive current control of PMSM EV drive using DSOGI-FLL based sliding mode observer," *IEEE Transactions on Industrial Electronics*, vol. 68, no. 7, pp. 5537–5547, 2021.

[20] H. Dan, P. Zeng, W. Xiong, M. Wen, M. Su, and M. Rivera, "Model predictive control-based direct torque control for matrix converter-fed induction motor with reduced torque ripple," *CES Transactions on Electrical Machines and Systems*, vol. 5, no. 2, pp. 90–99, 2021.

[21] M. Stender, O. Wallscheid, and J. Böcker, "Accurate torque control for induction motors by utilizing a globally optimized flux observer," *IEEE Transactions on Power Electronics*, vol. 36, no. 11, pp. 13261–13274, 2021.